JOURNAL OF CATALYSIS 134, 151–167 (1992)

A Study by *in situ* Laser Raman Spectroscopy of VPO Catalysts for *n*-Butane Oxidation to Maleic Anhydride

I. Preparation and Characterization of Pure Reference Phases

F. BEN ABDELOUAHAB,[1] R. OLIER,[1] N. GUILHAUME,[2] F. LEFEBVRE,[2] AND J. C. VOLTA[2]

[1]*Laboratoire de Physicochimie des Interfaces, Ecole Centrale de Lyon, 36 Avenue Guy de Collongue, B.P. 163, 69131 Ecully Cédex, France, and* [2]*Institut de Recherches sur la Catalyse, CNRS, 2 Avenue A. Einstein, 69626 Villeurbanne Cédex, France*

Received May 10, 1991

An *in situ* laser Raman spectroscopy (LRS) cell has been constructed in order to study the evolution of the local structure of the vanadium phosphate catalysts for *n*-butane oxidation to maleic anhydride in catalytic conditions. The LRS cell is described with the *on line* disposal for detection of the evolving gases. The first issue concerns the preparation and the physicochemical characterization of the reference phases of the VPO system: $(VO)_2P_2O_7$, α_{II}, β, γ, and δ $VOPO_4$. Their purity was controlled by X-ray diffraction and ^{31}P and ^{51}V solid NMR and their LRS spectra were studied in the 800–1200 cm^{-1} range characteristic of the P–O and V–O bonds. Among these phases only δ $VOPO_4$ is partly transformed (into α_{II} $VOPO_4$) in the catalytic conditions. From the evolution of their respective Raman spectra with temperature and with conditions of hydration, new proposals for the structure of γ $VOPO_4$ are given. They are in agreement with the solid state NMR data. Raman spectra of the phases exhibit features specific enough to allow identification of the different VPO structures.

INTRODUCTION

Laser Raman Spectroscopy (LRS) has been widely used to study oxide catalysts (*1–4*). An empirical correlation has been recently developed for relating Raman stretching frequencies of vanadium–oxygen (V–O) bonds to their bond lengths in vanadium oxide reference compounds (*4*). Due to the fact that the interference of gas phase spectra is negligibly weak, *in situ* Raman spectra of working catalysts at elevated pressures and temperatures can be obtained, thus making it possible to get information, during the activation of the catalyst, on the stability of the different phases present in the material. LRS studies were done on phosphorus–vanadium oxides (VPO) (*5–7*) which are used industrially for the oxidation of *n*-butane to maleic anhydride (*8, 9*). As has been previously shown (*5–7*), the interest in this technique stems from the fact that the spectrum of vanadyl pyrophosphate, $(VO)_2P_2O_7$, which is considered as the basic phase for this reaction, is highly different from that of β $VOPO_4$, which should play a catalytic role in the reaction pathway *n*-butane–maleic anhydride simultaneously with other $VOPO_4$ phases (*5*). Raman technique thus appears to be a very sensitive probe for the presence of $VOPO_4$-like impurities on $(VO)_2P_2O_7$. In reference (*5*), *in situ* Raman spectra for both β $VOPO_4$ and $(VO)_2P_2O_7$ at hydrocarbon oxidation conditions have been published. No development of new bands was detected, indicating a high stability of these two phases in catalytic conditions. In two other publications (*6, 7*), the same authors studied the role of lattice oxygen species using ^{18}O labeling of β $VOPO_4$. They concluded from their LRS experiments that the initial high activity of the catalyst was not associated with bulk catalyst reduction (*6*) and that the ini-

0021-9517/92 $3.00

tial interaction of *n*-butane with β $VOPO_4$ was fundamentally different from the initial interaction of olefins or oxygenated species (*7*). In fact, the vanadium–phosphorus oxide system is characterized by the facile formation and interconversion of a V(IV) phase, $(VO)_2P_2O_7$, and a number of V(V) phases, such as β $VOPO_4$ but also α_{II}, γ, and δ $VOPO_4$, in catalytic conditions and this has led to some confusion in the literature as to the detailed composition of the contact mass and the respective role of these phases in the reaction (*8*). We recently demonstrated the importance of the γ $VOPO_4$–$(VO)_2P_2O_7$ association for the best VPO catalysts (*10*). As a consequence, the LRS study of all $VOPO_4$ phases in catalytic conditions associated to a classical catalytic study in a differential reactor appeared to be very important for knowledge of the vanadium–phosphorus oxide system. This is particularly important for γ and δ $VOPO_4$, for which the structure and the Raman spectra are unknown.

The present publication describes results obtained by using LRS to examine VPO catalysts under reactions at high temperatures corresponding to those of industrial conditions. In this first paper, we describe the preparation and the physicochemical characterization of the pure VPO crystalline phases by XRD and ^{31}P and ^{51}V MAS NMR. Their evolution in the *in situ* LRS cell, in the *n*-butane/air atmosphere, and at the temperature of reaction, is described. A second paper will discuss catalytic results and the physicochemical evolution of a VPO catalyst prepared from $VO(HPO_4)$, 0.5 H_2O as studied in the *in situ* LRS cell in the same conditions. LRS informations obtained in catalytic conditions will be discussed in relation with results for butane oxidation to maleic anhydride.

CRYSTAL STRUCTURE KNOWLEDGE OF REFERENCE VPO PHASES

Diffraction patterns and proposals for the structure of $(VO)_2P_2O_7$ and $VOPO_4$ phases have been published elsewhere (*11*). If the structures of α_{II} $VOPO_4$ (*12*), β $VOPO_4$ (*13*), and $(VO)_2P_2O_7$ (*14*) are well known and have been refined, only structural models have been proposed for γ and δ $VOPO_4$ (*15*). The two forms γ and δ $VOPO_4$ would differ in the relative organization of the V–O–P layers (*11*).

EXPERIMENTAL

Preparation of Reference Phases

Pure VPO phases were prepared from the three precursors $VOPO_4 \cdot 2\ H_2O$, $NH_4(VO_2)_2PO_4$, and $VO(HPO_4) \cdot 0.5\ H_2O$. $VOPO_4 \cdot 2\ H_2O$ was prepared as described in Refs. (*16–18*) by heating V_2O_5 with 85% H_3PO_4 (P/V = 7) under reflux for 16 h. $NH_4(VO_2)_2PO_4$ was obtained according to Refs. (*18, 19*) by adding 85% H_3PO_4 to a solution of NH_4VO_3 10^{-2} *M* heated at 60°C (P/V = 1). $VO(HPO_4)$, 0.5 H_2O, which is known as the precursor of VPO catalysts, was prepared according to Ref. (*20*) by refluxing a suspension of V_2O_5 in isobutanol in the presence of 85% H_3PO_4 (P/V = 1.1).

After characterization of the precursors by X-ray diffraction, their decomposition was studied by Differential Thermal Analysis using a MDTA 85 SETARAM microanalyzer in order to determine the conditions of preparation of the VPO reference phases. Studies were conducted under nitrogen, oxygen, and air flows in the 25–800°C temperature range. Returned to room temperature, all products were collected and stored under dry argon to avoid rehydration.

$(VO)_2P_2O_7$ was obtained by dehydration of $VO(HPO_4)$, 0.5 H_2O under dry nitrogen at 475°C and 700°C for 6 h (heating rate 75°C. h^{-1}).

α_{II} $VOPO_4$ was prepared from $VOPO_4 \cdot 2\ H_2O$ by dehydration in dry air at 750°C for 17 h (heating rate 240°C h^{-1}).

β $VOPO_4$ was obtained by decomposition of $NH_4(VO_2)_2PO_4$ in dry air at 600°C for 10 h (heating rate 75°C h^{-1}).

γ $VOPO_4$ was prepared by oxydehydration of $VO(HPO_4)$, 0.5 H_2O at 680°C for 4 h under dry oxygen (heating rate 110°C h^{-1}).

δ $VOPO_4$ was obtained from $VO(HPO_4)$,

0.5 H_2O by oxydehydration in dry oxygen at 450°C for 168 h (heating rate 60°C h^{-1}). Increasing the temperature treatment up to 500°C during 61 h did not improve the crystallinity of the material.

With the exception of $(VO)_2P_2O_7$–475°C, these conditions led to well crystallized materials. Nevertheless, they were not optimized.

Conditions of preparation from the precursors were mostly in agreement with previous publications (*11, 18*). However, some discrepancies were observed in the case of the δ $VOPO_4$ phase preparation. Indeed, preparation in air from $VO(HPO_4)$ 0.5 H_2O as described in Ref. (*11*) led to a mixture of phases including $(VO)_2P_2O_7$.

Reference Phases and Catalyst Characterization

X-ray diffraction patterns of the pure phases before and after *in situ* LRS experiments were recorded with a Siemens diffractometer using Cu$K\alpha$ radiation.

The ^{31}P and ^{51}V NMR spectra were recorded on a Bruker MSL-300 spectrometer operating at 121.4 MHz for phosphorus and 78.86 MHz for vanadium. The ^{31}P NMR spectra were obtained under MAS conditions by use of a double bearing probehead while the ^{51}V ones were recorded under both static and MAS conditions. A single pulse sequence was used in all cases and the delays were chosen allowing the obtention of quantitative spectra (typically the pulse width was 2 ms (10°) and the delay was 10 to 100 s for phosphorus). The number of scans was 10 to 100 for phosphorus and 10,000 to 100,000 for vanadium (100 to 1000 under MAS conditions). The spectra were referred to external H_3PO_4 (85%) for phosphorus and $VOCl_3$ for vanadium.

A schematic diagram of the *in situ* cell, constructed at the Institut de Recherches sur la Catalyse and used for the Laser Raman study of the materials, is shown in Fig. 1. It was made of three stainless steel parts with different functions. The solid to be examined under reaction conditions was placed on the lower part on a sintered glass disc. 600 mg of VPO reference phase was generally used for each study. The temperature was controlled by a thermocouple in the centre of the catalyst powder. The reaction gases flew through the powder in the middle of this lower part which was heated by three thermoregulated fingers. The upper part held a glass window transparent to the laser beam. The gaseous effluent from the cell was analyzed by gas chromatography. The tightness of the cell was ensured by two gold wires. The composition and flow rate of the reacting gases (2.4% butane/air) were controlled by two flow meters. Experiments were done on a mass of 600 mg of solid with a flow rate of 3.6 liter h^{-1}. Detection of evolved gases

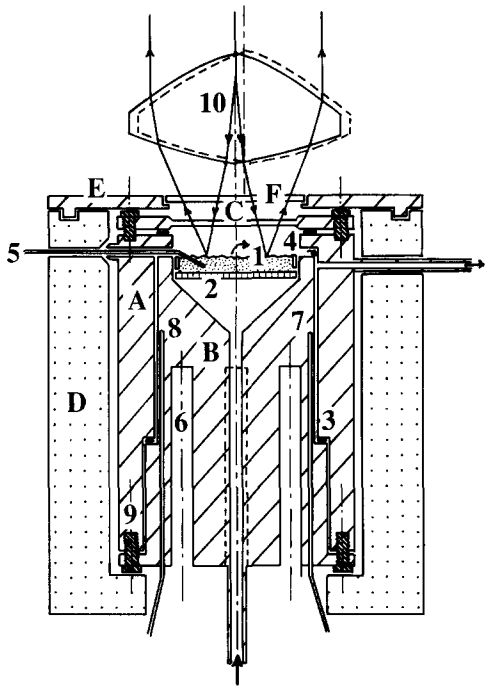

FIG. 1. (A) Chamber upper part; (B) chamber lower part; (C) glass window; (D) isolating shell; (E) thermal screen; (F) anticaloric filter; (1) catalyst; (2) sintered glass; (3 and 4) tightening rings; (5) temperature controller; (6) heating finger lodging; (7) chamber heating controller; (8) thermal security; (9) mounting bolts; (10) rotating lens.

was done by a FID detector from DELSI. CO and CO_2 were quantitatively transformed to CH_4 on a Raney Ni catalyst working at 300°C. It was thus possible to analyze all the gases with one FID detector. Two columns were used in parallel: a 1 m $\frac{1}{4}$ in. Porapak Q column to separate CO and CO_2, which are further transformed into CH_4, and a 3 m $\frac{1}{8}$ in. Lac 2R (13%)/H_3PO_4 (2.5%) on Gas ChromQ column to separate butane, acetic, and acrylic acids and maleic anhydride. The two columns were heated to 140°C. The tube connecting the cell to the chromatograph was heated to 120°C in order to avoid any condensation of the reaction products. Helium was the carrier gas.

Raman spectra were recorded on a DILOR OMARS 89 spectrophotometer equipped with an intensified photodiode array detector. The emission line at 514.5 nm from Ar^+ ion laser (Spectra Physics, Model 164) was used for excitation. The power of the incident beam on the sample was 36 mW. Time of acquisition was adjusted according to the intensity of the Raman scattering. From 30 to 100 spectra were accumulated in order to improve the signal-to-noise ratio. The wavenumber values obtained from the spectra were accurate to within about 2 cm^{-1}. To reduce both thermal and photodegradation of samples, the laser beam was scanned on the sample surface by means of a rotating lens in the same way as described in Ref. (*21*). The scattered light was collected in the back scattering geometry.

RESULTS

X Ray Spectra of Reference Phases

Figure 2 gives the spectra of $(VO)_2P_2O_7$ at 700°C (Fig. 2a), α_{II} $VOPO_4$ (Fig. 2b), β $VOPO_4$ (Fig. 2c), γ $VOPO_4$ (Fig. 2d), and δ $VOPO_4$ (Fig. 2e). They are in good agreement with previously published results (*14, 12, 13, 11, 11* respectively). The X ray patterns and indexation of the five phases are presented in Tables 1, 2, 3, 4, and 5 in the 0–45°, 2Θ domain.

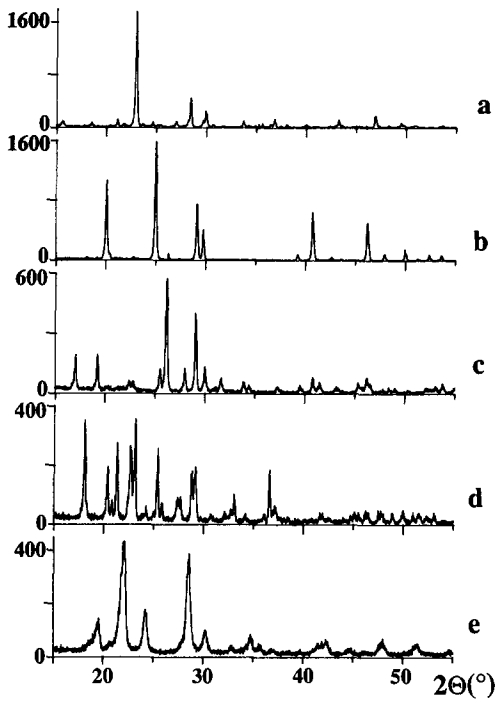

FIG. 2. X Ray spectra of the reference phases: (a) $(VO)_2P_2O_7$, 700°C; (b) α_{II} $VOPO_4$; (c) β $VOPO_4$; (d) γ $VOPO_4$; (e) δ $VOPO_4$.

^{31}P NMR Spectra of Reference Phases

Figure 3 gives the spectra of the $VOPO_4$ reference phases. Only one signal is observed at −20.5 ppm in the case of α_{II} $VOPO_4$ (Fig. 3a) and at −11.5 ppm in the case of β $VOPO_4$ (Fig. 3b). The width of the corresponding peaks is around 500–600 Hz and depends essentially on the crystallinity of the sample. These results are in agreement with the structures as determined by X-ray diffraction. Spectra of the two other phases, γ and δ $VOPO_4$ (Figs. 3c and 3d, respectively), appear to be more complex. γ $VOPO_4$ shows two principal signals at −17.3 and −21.2 ppm with the same relative intensity and a small signal evidenced by a shoulder at −14.9 ppm. δ $VOPO_4$ presents two signals at −8.4 and −17.6 ppm and a small peak around −6.5 ppm. The contribution of the three signals to the spectra is about 1/3/3 for the two phases. How-

TABLE 1

X-Ray Powder Pattern of $(VO)_2P_2O_7$

I/I_0	hkl	$2\Theta(°)$	d(Å)
3.55	012	14.135	6.261
4.12	111	15.650	5.658
3.73	020	18.505	4.791
1.83	113	21.700	4.092
100.00	200	23.005	3.863
1.83	201	23.615	3.764
1.83	211	25.430	3.500
4.94	212	26.995	3.300
25.73	024	28.450	3.135
4.12	213	29.640	3.012
13.48	032	29.945	2.981
1.76	115	30.700	2.910
0.98	222	31.630	2.826
5.27	016	33.705	2.657
1.29	133	34.245	2.616
1.13	125	34.965	2.564
3.02	034	35.615	2.518
2.70	230	36.415	2.465
1.18	040	37.475	2.398
2.86	232	38.040	2.364
2.03	233	40.000	2.252
0.84	117	40.920	2.204
0.84	143	42.430	2.129
6.07	323	43.230	2.091
1.90	044	43.595	2.074

TABLE 2

X-Ray Powder Pattern of α_{II} $VOPO_4$

I/I_0	hkl	$2\Theta(°)$	d(Å)
64.24	001	20.090	4.416
1.39	110	20.970	4.233
100.00	101	25.005	3.558
47.05	111	29.140	3.062
24.50	200	29.755	3.000
0.65	201	36.100	2.486
4.89	211	39.215	2.295
38.20	002	40.710	2.214
2.27	220	42.560	2.122
0.96	300	43.540	2.077
30.83	112	46.195	1.964
5.00	310	47.865	1.899
8.35	301	49.960	1.824

ever, for the first peak corresponding to phosphorus in lower extent, this contribution was different depending on the conditions of treatment of the phases. As an example, it disappeared almost completely after treatment of γ $VOPO_4$ under reactional conditions. As a consequence, it was postulated that it corresponded to another phosphate compound occurring as an impurity and not to phosphorus atoms of the γ and δ $VOPO_4$ structures.

^{51}V *NMR Spectra of the Reference Phases*

Figure 4 gives spectra of the reference phases in static conditions. For β, γ, and δ $VOPO_4$ (Figs. 4b, 4c, and 4d), spectra are very similar and show essentially peaks at about -354, -300, and -284 ppm, respectively. They are quite similar to the spectrum of V_2O_5 for which a signal of the same type is observed at -297 ppm. This is in favour of an octahedral coordination of vanadium, in agreement with the structure of β $VOPO_4$ (*13*) and the proposed structures for γ and δ $VOPO_4$ (*15*). For α_{II} $VOPO_4$, the spectrum is more complex with three maxima at -77, -316, and -592 ppm indicating that several phenomena are superimposed (anisotropy, quadrupolar interaction . . .).

TABLE 3

X-Ray Powder Pattern of β $VOPO_4$

I/I_0	hkl	$2\Theta(°)$	d(Å)
29.63	101	17.050	5.196
28.26	011	19.275	4.601
7.76	111	22.405	3.965
6.84	200	22.800	3.897
17.80	002	25.540	3.485
100.00	201	26.170	3.402
15.07	102	28.070	3.176
64.95	020	29.095	3.067
19.26	211	30.020	2.974
10.83	112	31.615	2.828
8.97	121	33.880	2.644
5.78	202	34.405	2.605
5.39	220	37.250	2.412
5.00	221	39.485	2.280

TABLE 4

X-Ray Powder Pattern of γ $VOPO_4$

I/I_0	hkl	$2\Theta(°)$	d(Å)
12.12	102	14.330	6.176
100.00	031	18.100	4.897
51.59	032	20.415	4.347
15.39	202	20.850	4.257
73.33	004	21.370	4.155
69.60	221	22.655	3.922
98.90	040	23.160	3.837
67.77	230	25.400	3.504
14.11	213	25.895	3.438
23.64	223	27.695	3.218
48.46	105	28.800	3.097
51.59	311	29.160	3.060
5.38	312	30.745	2.906
8.25	152	32.135	2.783
11.36	144	32.715	2.735
25.84	106	33.090	2.705
6.74	332	34.180	2.621
6.46	333	36.065	2.488
50.80	161	36.610	2.453
15.82	341	37.175	2.417
3.96	226	38.460	2.339
6.74	146	41.615	2.168

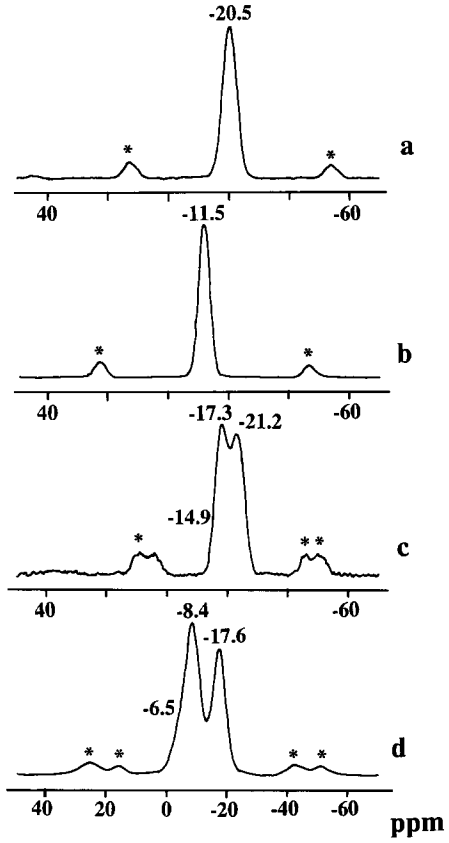

FIG. 3. ^{31}P NMR spectra of the reference phases: (a) α_{II} $VOPO_4$; (b) β $VOPO_4$; (c) γ $VOPO_4$; (d) δ $VOPO_4$. *Rotating bands.

Figure 5 shows a small part of the ^{51}V MAS NMR spectra of the reference phases. Indeed, all spectra correspond to vanadium in octahedral coordination and, so, spinning side-bands are present on all the frequency range of the experiments. However, in this case also, as for the ^{31}P NMR spectra, it is possible to separate the four $VOPO_4$ phases into two groups: first, the α_{II} and β $VOPO_4$ (Figs. 5a and 5b), which give only one peak and second, the γ and δ $VOPO_4$ (Figs. 5c and 5d), which give at least three peaks. The spectra of these two latter phases are in favour of the existence of, at least, three different vanadium atoms in both structures. One of them should correspond to the impurity previously postulated in the ^{31}P NMR study.

TABLE 5

X-Ray Powder Pattern of δ $VOPO_4$

I/I_0	hkl	$2\Theta(°)$	d(Å)
24.24	002	19.580	4.530
100.00	111	22.080	4.023
36.00	012	24.165	3.680
85.21	020	28.550	3.124
18.56	021	30.260	2.951
4.86	013	32.770	2.731
13.26	022	34.785	2.577
4.86	—	35.700	2.513
2.69	—	36.925	2.432
2.69	—	39.690	2.269
7.67	104	41.455	2.176
11.46	—	42.455	2.127
4.21	—	44.660	2.027

LRS Spectra of the Reference Phases

Figures 6 to 8 give the LRS spectra of reference phases.

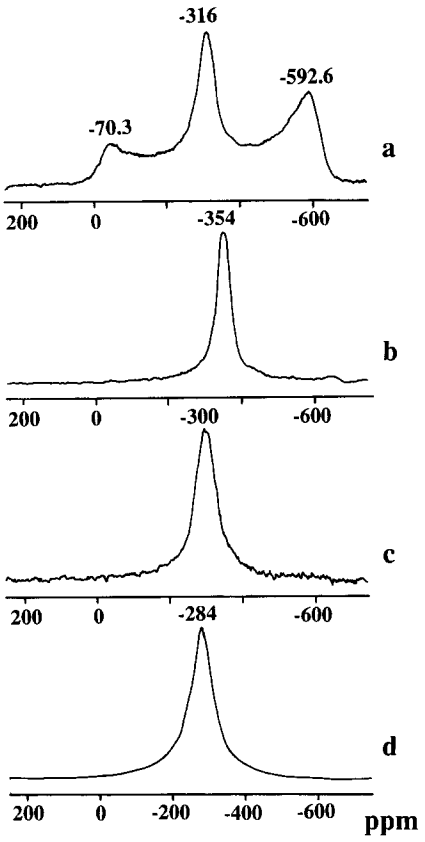

FIG. 4. ^{51}V NMR spectra of the reference phases: (a) α_{II} $VOPO_4$; (b) β $VOPO_4$; (c) γ $VOPO_4$; (d) δ $VOPO_4$ (static conditions).

In Fig. 6 are shown spectra of $VO(HPO_4) \cdot 0.5\ H_2O$ (Fig. 6a), precursor for the synthesis of $(VO)_2P_2O_7$ and VPO catalysts, α_I $VOPO_4$ (Fig. 6b) and $VOPO_4 \cdot 2\ H_2O$ (Fig. 6c). α_I $VOPO_4$ and $VOPO_4 \cdot 2\ H_2O$ appear to be phases of minor interest in catalysis but their spectra exhibit some features useful for discussion. The precursor spectrum was obtained after a thermal treatment at 300°C for 12 h under nitrogen, which led to a marked decrease in sample fluorescence, allowing the Raman bands to emerge. Figure 7 shows spectra of vanadyl pyrophosphate, $(VO)_2P_2O_7$, well and poorly crystallized, prepared at two different temperatures. Figure 8 shows spectra of α_{II}, β, γ, and δ $VOPO_4$, vanadium (V) phases of major interest in catalysis. Wavenumbers of the Raman bands of the corresponding phases are listed in Tables 6 to 13.

All the vanadium (V) phase spectra exhibit two distinct ranges, below 700 cm^{-1} (range 1) and between 850 and 1200 cm^{-1} (range 2). Range 1 relates to bending modes, coupled vibrations, and collective modes of the crystal lattice. Range 2 relates to stretching modes of P–O and V–O bonds. Main bands are always in this wavenumber range. The aim of this paper being to study phase evolution between room temperature and catalytic reaction conditions, we chose to use this peculiar range as it was possible to record it in a single shot. Thus our discussion will be limited to the range 800–1200 cm^{-1}.

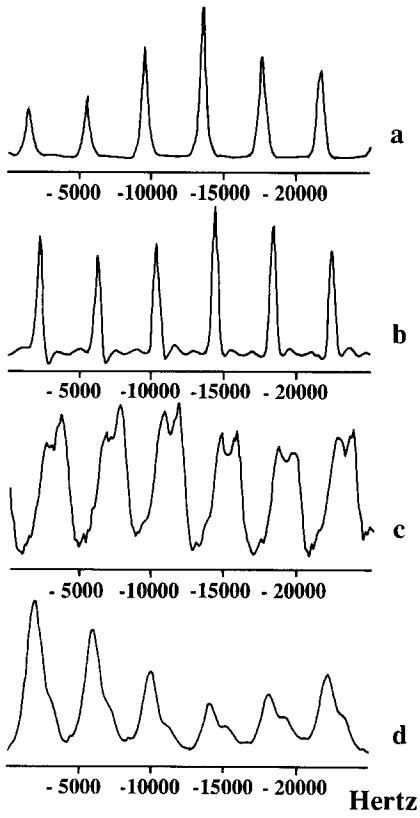

FIG. 5. ^{51}V MAS NMR spectra of the reference phases: (a) α_{II} $VOPO_4$; (b) β $VOPO_4$; (c) γ $VOPO_4$; (d) δ $VOPO_4$ (rotating conditions).

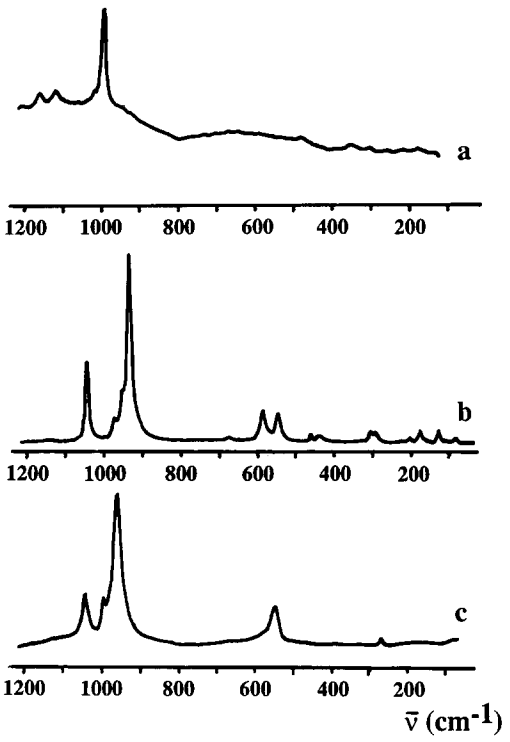

FIG. 6. Raman spectra of some reference phases: (a) $VO(HPO_4) \cdot 0.5\ H_2O$; (b) $\alpha_I\ VOPO_4$; (c) $VOPO_4 \cdot 2\ H_2O$.

Among these phases, only three had been previously studied by Raman spectroscopy: $(VO)_2P_2O_7$ (*5*), α_{II} $VOPO_4$ (*22*), and β $VOPO_4$ (*5–7, 22*). Despite some discrepancies, particularly in the low energy part of the spectra, our results are in good agreement with previous works. Main bands of $(VO)_2P_2O_7$ have been assigned to ν_{as} (P–O–P) vibration (*5*). The splitting into two bands may be attributed to two different kinds of pyrophosphate with different P–O–P angles, as determined in Ref. (*14*). For α_{II} and β $VOPO_4$, the situation is far less clear as some discrepancies exist in the literature. The controversy is mainly on two points:

First, how far can we use the simplifying hypothesis of independent vibrations of atomic groups such as V–O or PO_4 (*7*)? It seems to us that given the peculiar structure of all these phases resulting from the combination of tetrahedra and highly distorted octahedra, the V–O short bond may be treated as an isolated vibration only weakly coupled with others. As a consequence, it would be possible to link the bond length to the wavenumber of vibration, as suggested in Ref. (*4*).

Second, which band can be assigned to the V–O short bond stretching mode? Owing to the fact that in nearly all of these compounds the V–O short bond is—when known—about 1.58 Å, as in crystalline V_2O_5 (*23, 24*), the corresponding Raman band should appear in the range 990–1000 cm^{-1} (Table 14), in contradiction to the assignment made in Refs. (*25, 26*) at 944 cm^{-1} on the basis of normal coordinate analysis but in agreement with other works (*5–7, 22*). Nevertheless, in spite of this contradictory assignment, all these works lead to the common conclusion that Raman bands are only rarely attributable to a unique vibration but involve coupling.

Figures 9 to 14 show the spectra for reference phases when temperature increases

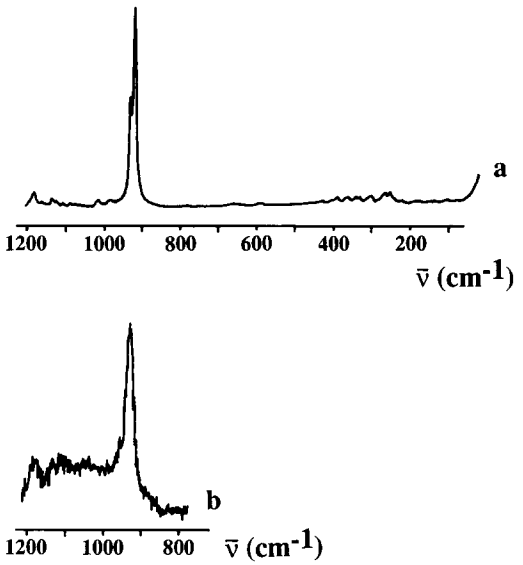

FIG. 7. Raman spectra of the $(VO)_2P_2O_7$ phases: (a) well crystallized material ($VO(HPO_4) \cdot 0.5\ H_2O$ calcined at 700°C); (b) poorly crystallized material ($VO(HPO_4) \cdot 0.5\ H_2O$ calcined at 475°C).

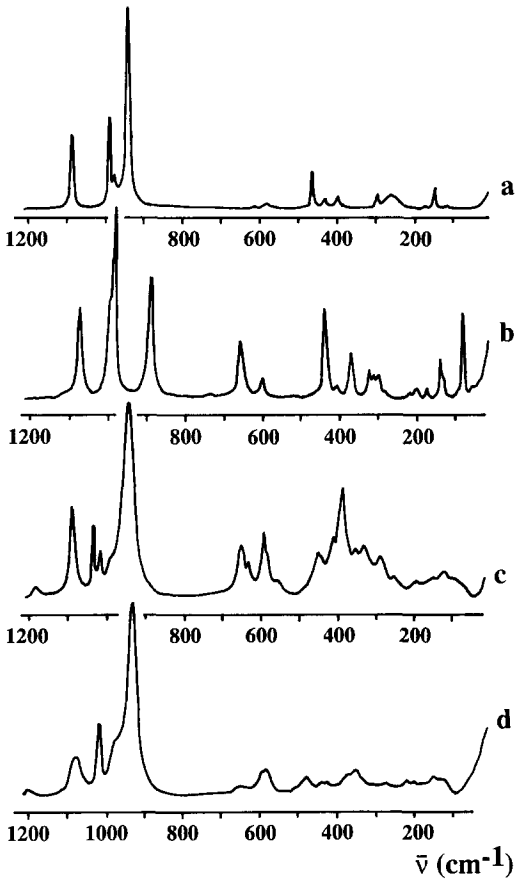

FIG. 8. Raman spectra of the $VOPO_4$ phases: (a) α_{II} $VOPO_4$; (b) β $VOPO_4$; (c) γ $VOPO_4$; (d) δ $VOPO_4$.

from 25°C up to 420–440°C under *n*-butane/air flow (catalytic conditions). Figure 15 allows a direct comparison of the spectra of the phases of interest in catalysis at the reaction temperature. This figure evidences that Raman spectra are able to give information on *in situ* VPO catalysts. Spectra of the different phases exhibit features specific enough to allow identification of phases even in a mixture and even if identification is sometimes difficult due to the bad signal/noise ratio.

For α_{II}, β and γ $VOPO_4$, there is no evolution of the spectra with increasing temperature in the reactional atmosphere (Figs. 9–11). In contrast, as can be noted in Fig. 12, the δ $VOPO_4$ phase shows a peculiar

TABLE 6

Raman Peaks of $VO(HPO_4)\cdot 0.5\,H_2O$ at Room Temperature

$\bar{\nu}$ (cm^{-1})	$\bar{\nu}$ (cm^{-1})
1204 vW	467 W
1156 W	341 W
1113 W	291 vW
1010 W, sh	204 vW
988 S	162 vW

Note. S: Strong; W: Weak; vW: very Weak; sh: shoulder.

behavior: during the temperature rise to 440°C and during the first hours at that temperature, its spectrum is not far from the one obtained under air, but after about 15 h at 440°C, a new band appears at 994 cm^{-1}, whose relative intensity increases as temperature is lowered. This band might be due to α_{II} or β $VOPO_4$. As there was no band either at 894 or at 1064 cm^{-1} (as in β at 440°C), the presence of β $VOPO_4$ in the sample could be ruled out, giving evidence that δ $VOPO_4$ under catalytic conditions is partly transformed into α_{II} $VOPO_4$. This was confirmed by examination of the sample *ex situ* after the LRS study by XRD and ^{31}P NMR.

TABLE 7

Raman Peaks of α_I $VOPO_4$ at Room Temperature

$\bar{\nu}$ (cm^{-1})	$\bar{\nu}$ (cm^{-1})
1143 W	433 W, br
1038 S	302 M
965 M	293 M
944 M	225 W
928 vS	197 M
905 W, sh	171 M
663 W, br	125 M
579 S	102 vW
541 S	79 M
458 M	

Note. vS: very Strong; S: Strong; M: Medium; W: Weak; vW: very Weak; sh: shoulder; br: broad.

TABLE 8

Raman Peaks of $VOPO_4 \cdot 2\ H_2O$ at Room Temperature

$\bar{\nu}$ (cm^{-1})	$\bar{\nu}$ (cm^{-1})
1038 M	451 vW
989 M	279 M
954 vS	201 W
658 W	144 W
542 M	84 W

Note. vS: very Strong; M: Medium; W: Weak; vW: very Weak.

TABLE 10

Raman Peaks of α_{II} $VOPO_4$ at Room Temperature

$\bar{\nu}$ (cm^{-1})	$\bar{\nu}$ (cm^{-1})
1091 S	466 M
993 S	433 M
979 M	399 M
945 vS	300 M
650 vW	265 M, br
619 W	177 W
587 W	149 M
550 vW	118 W

Note. vS: very Strong; S: Strong; M: Medium; W: Weak; vW: very Weak; br: broad.

DISCUSSION OF RESULTS

Among the V(V) phases α_I, α_{II}, and β $VOPO_4$ and $VOPO_4 \cdot 2\ H_2O$ are the only phases whose structures had been determined (*12, 13, 27, 28*). $(VO)_2P_2O_7$ structure has also been published (*14*). For γ and δ $VOPO_4$, as only structure proposals had been advanced (*15*), we will try to provide new information, taking into account our knowledge of the best known $VOPO_4$ phase structures and the evolution of the Raman spectra of all these phases with some parameters (such as temperature and hydration).

TABLE 9

Raman Peaks of Well Crystallized $(VO)_2P_2O_7$ at Room Temperature

$\bar{\nu}$ (cm^{-1})	$\bar{\nu}$ (cm^{-1})
1215 vW	465 vW
1196 W, sh	449 vW
1186 M	429 W
1168 vW	407 vW
1153 vW	391 W
1138 W	363 W
1126 W	343 W
1110 vW	330 W
1090 W	317 vW, sh
1073 W,br	304 W
1020 W	269 M
985 W	253 M
933 S	221 W
921 vS	191 W
894 vW, sh	181 W
654 W	151 W
597 W	136 W
583 vW	106 W, br
486 vW	80 W

Note. vS: very Strong; S: Strong; M: Medium; W: Weak; vW: very Weak; sh: shoulder; br: broad.

TABLE 11

Raman Peaks of β $VOPO_4$ at Room Temperature

$\bar{\nu}$ (cm^{-1})	$\bar{\nu}$ (cm^{-1})
1110 vW	368 M
1075 S	320 M
997 M, sh	309 M
986 vS	295 M
892 S	280 W
804 vW	226 vW
782 vW	214 W
741 vW	199 W
656 M	170 W
599 M	134 M
465 vW, sh	127 W, sh
435 S	88 vW, sh
406 W	78 S

Note. vS: very Strong; S: Strong; M: Medium; W: Weak; vW: very Weak; sh: shoulder.

TABLE 12

Raman Peaks of γ $VOPO_4$ at Room Temperature

$\bar{\nu}$ (cm^{-1})	$\bar{\nu}$ (cm^{-1})
1188 M	454 M
1096 S	416 W, sh
1040 S	390 S
1022 M	358 vW
996 W, sh	334 M
958 M, sh	293 M
951 vS	255 vW
656 S	196 vW
638 W, sh	151 vW
596 S	123 W
556 W	

Note. vS: very Strong; S: Strong; M: Medium; W: Weak; vW: very Weak; sh: shoulder.

Structural Features of VPO Phases from Literature

First of all, let us recall some important features about the structure of these phases.

α_I, α_{II}, and β $VOPO_4$, as well as $VOPO_4 \cdot 2\ H_2O$ and $(VO)_2P_2O_7$ are built with VO_6 octahedra and PO_4 tetrahedra. Octahedra are distorted and exhibit a short vanadium–oxygen bond (V=O) and a long vanadium–oxygen bond (V–O). The other four oxygen atoms can be described as equatorial oxygens and the V–O equatorial bond length is intermediate between short and long bonds.

In the case of $(VO)_2P_2O_7$, the VO_6 octahedra are two by two coupled by an edge (two octahedra sharing two equatorial oxygens) orthogonal to the V=O short bond. Moreover, octahedra form chains along the alternate short and long V–O bonds. Each PO_4 tetrahedron shares an oxygen with another tetrahedron to form the pyrophosphate group. A second oxygen is shared between one tetrahedron and the two vanadium atoms of the coupled octahedra. The other two oxygen atoms are shared with octahedra belonging to different chains.

For the α $VOPO_4$ phases as well as for β $VOPO_4$, the octahedra also form chains with alternate short and long vanadium–oxygen bonds. Perpendicular to the general chain direction, the octahedra are linked to PO_4 tetrahedra. In the case of $VOPO_4 \cdot 2\ H_2O$, there is no chain as long V–O bonds are replaced by $V–OH_2$ bonds.

The β $VOPO_4$ phase differs from the others in that two oxygen atoms of each PO_4 are shared with two octahedra belonging to the same chain (that is a specificity of β $VOPO_4$), while the other two oxygen atoms are shared with octahedra from different chains (as in $(VO)_2P_2O_7$)).

TABLE 13

Raman Peaks of δ $VOPO_4$ at Room Temperature

$\bar{\nu}$ (cm^{-1})	$\bar{\nu}$ (cm^{-1})
1200 vW	444 vW
1090 M	428 vW
1075 M	376 vW, br
1020 M	352 W
977 W, sh	276 vW, br
936 S	223 W
655 W	153 W
590 M, br	108 W
482 W	

Note. S: Strong; M: Medium; W: Weak; vW: very Weak; br: broad.

TABLE 14

Comparison between Bond Lengths and Possible Assignments of Raman Bands to V–O Structures

Phases	Bond length (Å)	Raman shift (cm^{-1})
V_2O_5	1.58	996
$VOHPO_4 \cdot 0.5\ H_2O$	1.57	988
$VOPO_4 \cdot 2\ H_2O$	1.567	989
α_I $VOPO_4$	1.58	—[b]
α_{II} $VOPO_4$	1.58	993
β $VOPO_4$	1.57	997
γ $VOPO_4$[a]	—	—
δ $VOPO_4$[a]	—	—
$(VO)_2P_2O_7$	1.53–1.55	985

[a] Structures yet unknown.

[b] No band is observed in the 980–1000 cm^{-1} range.

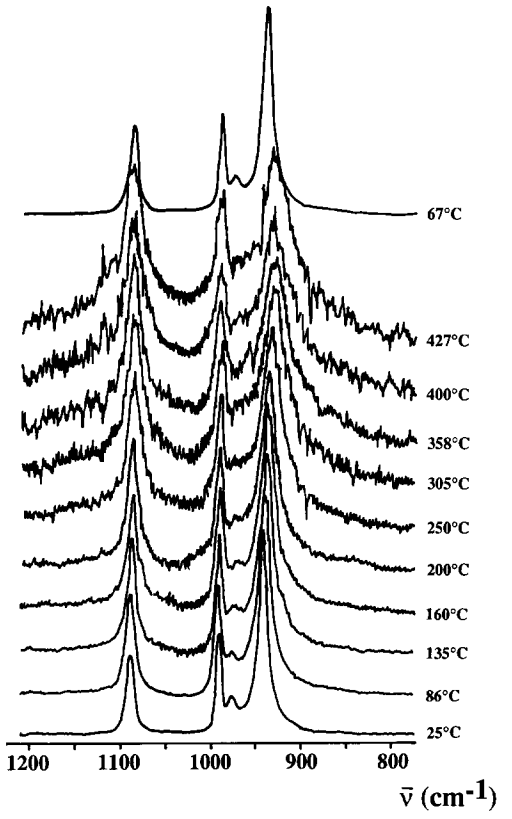

FIG. 9. Evolution of the spectrum of α_{II} $VOPO_4$ under catalytic atmosphere with increasing temperature (2.4% butane/air).

In contrast, for α_I and α_{II} $VOPO_4$ and $VOPO_4 \cdot 2\ H_2O$, oxygen atoms from any PO_4 tetrahedron are shared with octahedra from different chains. It follows that the $V-O_{equatorial}-P$ links are all identical for α_I $VOPO_4$. The same assumption is valid for α_{II} $VOPO_4$ and $VOPO_4 \cdot 2\ H_2O$. For β $VOPO_4$ we can identify three different kinds of $V-O_{equatorial}-P$ links with different angles, only one of them being of the same kind as in the previously described phases (it occurs twice in each octahedron). It is worth noting that the main difference between α_I and α_{II} $VOPO_4$ structures is the inversion in position of the vanadium and phosphorus atoms relative to the equatorial plane: V and P are on the same side for α_I $VOPO_4$ (and for $VOPO_4 \cdot 2\ H_2O$) and on opposite sides for α_{II} $VOPO_4$. The V=O short bond never intersects the equatorial plane. According to Ref. (*27*), in the α phases, the vibration amplitude of the V atom along the V=O direction is large and can lead to a change of its position inside its octahedron with only slight other modifications.

Connection between Structures and Raman Band Assignments

α_I and α_{II} $VOPO_4$ and $VOPO_4 \cdot 2\ H_2O$ exhibit layered structures (*27*). Unlike β $VOPO_4$, α_I and α_{II} $VOPO_4$ can be easily hydrated. We established that the final hydration product is in both cases the dihydrate $VOPO_4 \cdot 2\ H_2O$ whose structure exhibits the same V and P relative positions as in the α_I $VOPO_4$ phase (*28*). Dehydration of $VOPO_4 \cdot 2\ H_2O$ always leads to the α_I $VOPO_4$ phase (at temperatures below about 750°C). We also noted that γ and δ $VOPO_4$

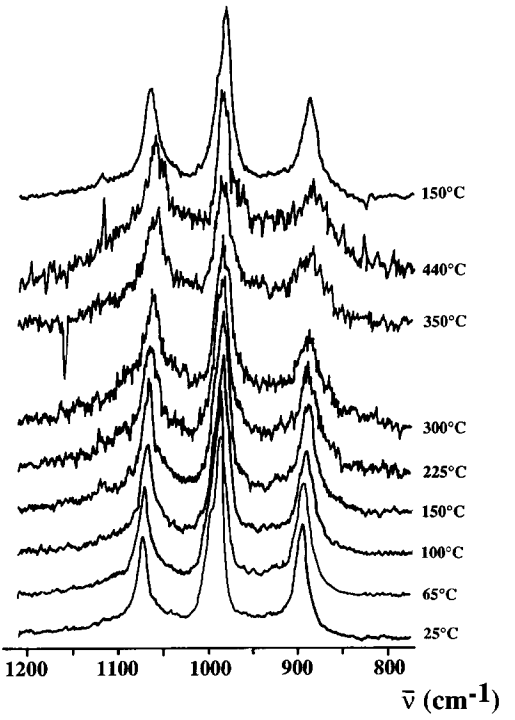

FIG. 10. Evolution of the spectrum of β $VOPO_4$ under catalytic atmosphere with increasing temperature (2.4% butane/air).

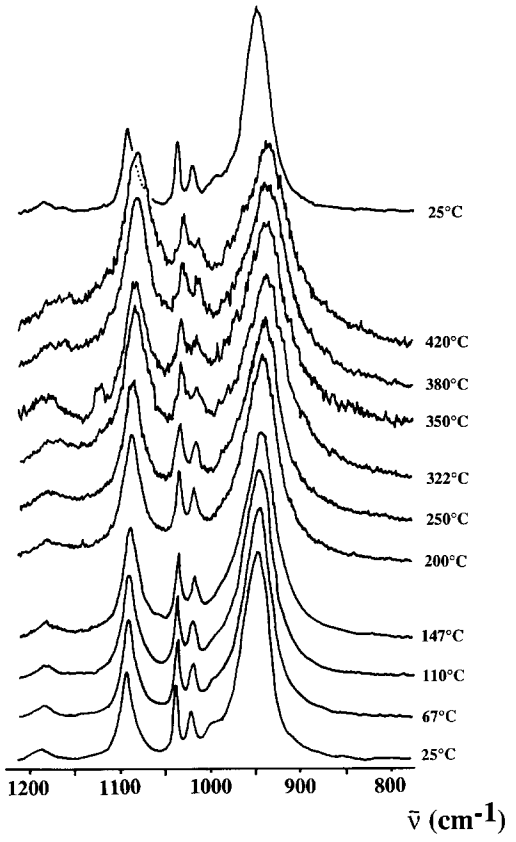

FIG. 11. Evolution of the spectrum of γ $VOPO_4$ under catalytic atmosphere with increasing temperature (2.4% butane/air).

phases are easily hydrated too, leading to the same final product $VOPO_4 \cdot 2\ H_2O$ (*29*) in a time (3 h) intermediate between those necessary for α_I (0.75 h) and α_{II} (10 h) under a saturated atmosphere at room temperature (about 20°C). When hydration was continued by adding a drop of liquid water on the $VOPO_4 \cdot 2\ H_2O$ samples, the main band sharpened and shifted toward the position 934 cm^{-1} of the ν_s (PO_4^{3-}) band in solution (*30*). Taking into account the fact that—when they are known—the four P–O bond lengths are nearly identical in this series of phosphates, it seems then logical to assign to the symmetric stretching ν_s (PO_4^{3-}) the following bands: 928 cm^{-1} (α_I), 945 cm^{-1} (α_{II}), 951 cm^{-1} (γ), 936 cm^{-1} (δ), and 954 cm^{-1} ($VOPO_4 \cdot 2\ H_2O$). The assumption of equivalent P–O distances is not valid for β $VOPO_4$ (*13*), but even in that case, the distortion is negligibly small.

Incidentally, we also tried to intercalate other molecules than water in the α_I $VOPO_4$ structure. An α_I $VOPO_4$ sample was exposed to NH_3 in a sealed bulb. After this treatment, the sample was left under a dry air flow at room temperature in order to ease the ammonia evolution. Changes in the Raman spectrum are observed within the first 10 min, after which no further modification can be detected (*29*). Main bands are then located at 928, 943, 964, 975, 992, 1023, 1037, and 1091 cm^{-1}. Spectrum analysis shows that it results from a combination of α_I, α_{II}, γ, and δ $VOPO_4$ spectra; i.e., all

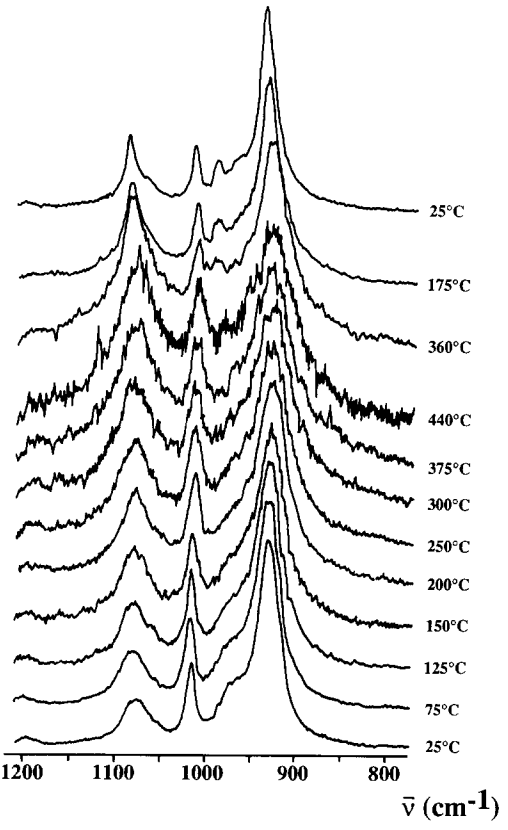

FIG. 12. Evolution of the spectrum of δ $VOPO_4$ under catalytic atmosphere with increasing temperature (2.4% butane/air).

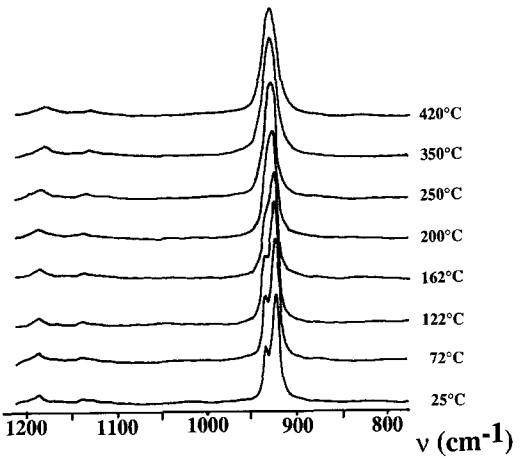

FIG. 13. Evolution of the spectrum of well crystallized $(VO)_2P_2O_7$ under catalytic atmosphere with increasing temperature (2.4% butane/air).

$VOPO_4$ phases with the notable exception of β $VOPO_4$. Only the 964 cm^{-1} band remains unexplained.

From these results we can thus infer that γ and δ $VOPO_4$ are built with the same structural elements as α_I and α_{II} $VOPO_4$ and possess a layered structure.

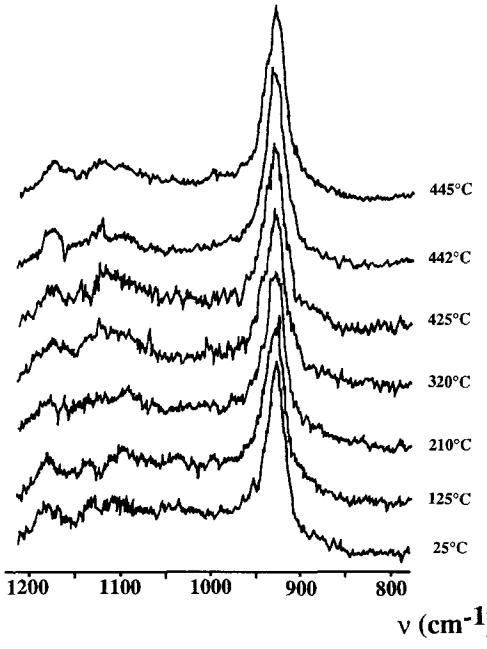

FIG. 14. Evolution of the spectrum of poorly crystallized $(VO)_2P_2O_7$ under catalytic atmosphere with increasing temperature (2.4% butane/air).

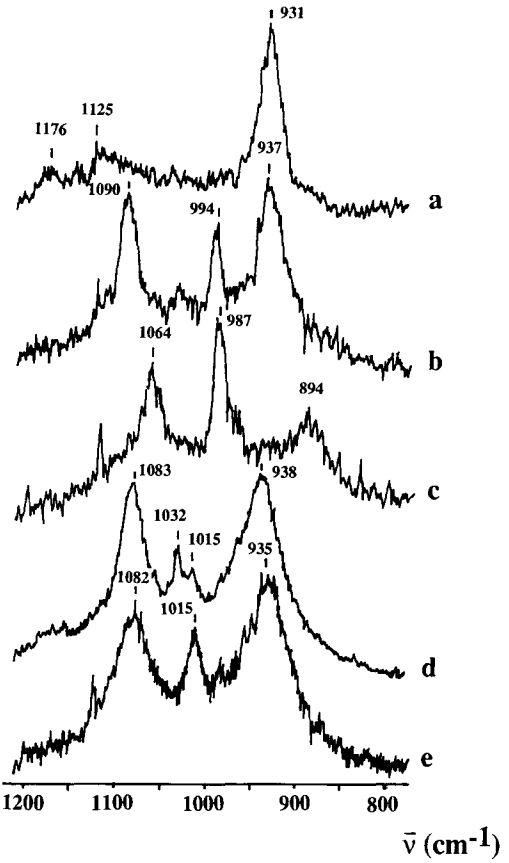

FIG. 15. LRS spectra of the reference phases at 430°C under catalytic atmosphere (2.4% butane/air): (a) poorly crystallized $(VO)_2P_2O_7$; (b) α_{II} $VOPO_4$; (c) β $VOPO_4$; (d) γ $VOPO_4$; (e) δ $VOPO_4$.

In recent papers, Lashier *et al.* (*6, 7*) studied $(VO)_2P_2O_7$ oxidation to β $VOPO_4$ with $^{18}O_2$ as well as $^{16}O_2$ by Raman spectroscopy. The authors give interesting informations about Raman band assignment using the structural relations between $(VO)_2P_2O_7$ and β $VOPO_4$. Comparison of $(VO)_2P_2O_7$ and β $VOPO_4$ structures clearly show that it is

(i) the oxygen atoms engaged in the pyrophosphate group and

(ii) the oxygen atoms shared by one tetrahedron and two octahedra that are directly involved in the oxidation process of

$(VO)_2P_2O_7$, while oxygen atoms shared with octahedra from different chains remain nearly unaffected (as well as the oxygen atom linked to vanadium through the V=O short bond).

They showed that the 998 cm^{-1} band (assigned to $\nu_{V=O}$) remains unaffected by the particular isotope used in the oxidation process while two of the three other main bands (896, 987 cm^{-1}) are split, revealing that the corresponding vibrations involve ^{16}O or ^{18}O depending on the oxidation conditions. As shown by the authors, the three bands at 896, 987, and 1072 cm^{-1} can be assigned to $V-O_{equatorial}-P$ coupled stretching vibrations. The most energetic vibration (1072 cm^{-1}) remains nearly unaffected and must then be due to the vibration of the particular kind of oxygen atom not engaged in the link between octahedra of the same chain, i.e., the peculiar feature common with α_I and α_{II} $VOPO_4$ and $VOPO_4 \cdot 2\ H_2O$. Given the analogies between the structures, we assume that this peculiar vibration will be visible in the α_I and α_{II} $VOPO_4$ phase spectra at an energy of the same order of magnitude as in β $VOPO_4$. Moreover we noted that several bands exhibited similar behaviour during our study of the Raman spectra as a function of temperature. The 1072 cm^{-1} band in the β $VOPO_4$ spectrum intensifies relative to the main band (987 cm^{-1}) as temperature increases. As the bands at 1040 cm^{-1} in α_I, 1090 cm^{-1} in α_{II}, 1040 and 1090 cm^{-1} in γ, and 1075 and 1090 cm^{-1} in δ $VOPO_4$ exhibit the same temperature dependence we were tempted to consider that these bands are related to the same kind of vibration: $V-O_{equatorial}-P$ coupled stretching.

The shift in wavenumbers observed between phases may thus result from differences in the V–O–P angle. As a matter of fact, this band is shifted to higher energy with an increased value of the angle (Table 15). If we use this assumption as a guideline, we are led to the conclusion that γ and δ $VOPO_4$, which exhibit the 1090 cm^{-1} band, must have the same V–O–P chains as α_{II} $VOPO_4$ and, moreover, that γ $VOPO_4$, owing to the band at 1040 cm^{-1}, must also possess V–O–P chains as in α_I $VOPO_4$, while δ, which exhibits a band at 1075 cm^{-1}, must possess chains as in β $VOPO_4$.

TABLE 15

Correspondence between V–O–P Bond Angle and Raman Shift

Phases	V–O–P angle (°)	Raman shift (cm^{-1})[a]
α_I $VOPO_4$, $VOPO_4 \cdot 2\ H_2O$	133.7	1040
α_{II} $VOPO_4$	151	1090
β $VOPO_4$	142.5	1075
γ $VOPO_4$	?[b]	1040, 1096
δ $VOPO_4$	?[b]	1075, 1090

[a] Raman shift corresponding to P–O, $V-O_{equatorial}$ stretching coupled modes.

[b] Structures yet unknown.

Proposed Structural Scheme for γ $VOPO_4$

Previous considerations give us a clue to propose a structure for γ $VOPO_4$ which is presented in Fig. 16. It differs radically from that given in Ref. (*15*). The situation seems to be far more intricate for δ $VOPO_4$ and, at this moment, we are not able to suggest any structure, but we assume that it must be a layered one, taking into account its capability for hydration.

From Fig. 12, it can be inferred that in catalytic conditions (2.4% butane/air—T = 440°C) the δ $VOPO_4$ phase is partly transformed into α_{II} $VOPO_4$. We think that a thermodynamic equilibrium between these two phases is reached. We postulate that it should depend on temperature and butane/air ratio.

Taking into account the specific features for ^{31}P NMR (Figs. 3c and 3d) and for ^{51}V MAS NMR (Figs. 5c and 5d) of γ and δ $VOPO_4$, it can be inferred that two kinds of P and V atoms exist in these two phases. This appears to be partly in agreement with LRS results where it can be seen that Raman shifts at 1040 and 1090 cm^{-1} (γ $VOPO_4$) and 1075 and 1090 cm^{-1} (δ $VOPO_4$) (see Table

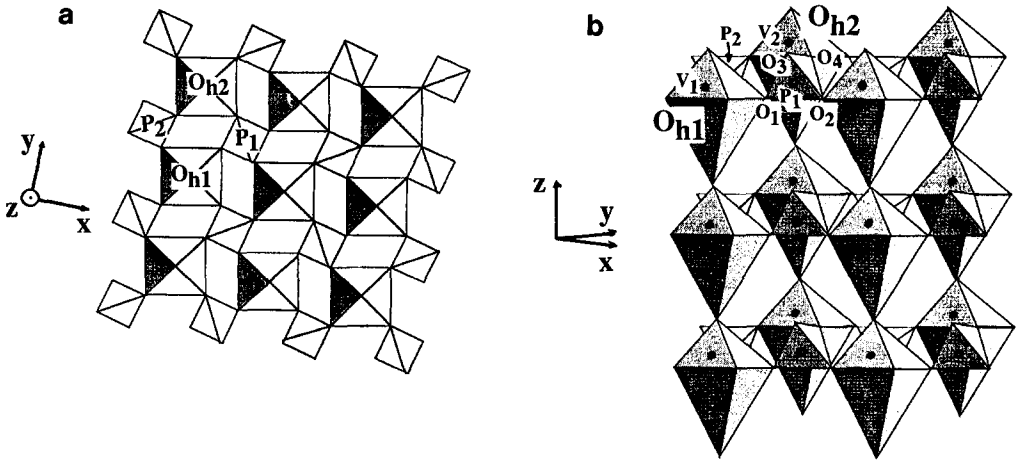

FIG. 16. Structural proposals for γ $VOPO_4$ (from the LRS study): (a) in the (001) plane; (b) along the 100 direction. Short V=O bonds are situated on the same side of the equatorial plane of the VO_6 octahedra.

15) should correspond to two different V environments as is observed in Fig. 16 for the proposed structure of γ $VOPO_4$. In this structure, short V=O bonds are such that vanadium and oxygen atoms are both located above the equatorial oxygen planes and are all in the $\pm z$ direction, contrary to α_I and α_{II} $VOPO_4$ in which nearest neighbours V–O short bonds are always in *trans* position. Considering octahedra O_{h_1} and O_{h_2} linked by two identical PO_4 tetrahedra, oxygen atoms O_1 and O_2 are located in the equatorial plane of O_{h_1} while O_3 and O_4 are located in the equatorial plane of O_{h_2}. It should be noted that O_{h_2} is shifted upwards (in the $\pm z$ direction) with respect to O_{h_1}. The phosphorus atom P_1 can be seen above the equatorial plane of O_{h_1} on the same side as vanadium atom V_1 giving evidence of α_I $VOPO_4$ type chains. It is also under the equatorial plane of O_{h_2} on the opposite side of this plane with respect to vanadium atom V_2. In this case, the link is of the α_{II} $VOPO_4$ type. For O_{h_1}, all the links are of the α_I type, while they are all of the α_{II} type for O_{h_2}.

Owing to the fact that ^{31}P NMR of γ $VOPO_4$ shows at least two different P environments, we can infer that the real structure of this phase (two oxygen atoms link in the α_I mode, the other two in the α_{II} mode) would result from PO_4 distortion around the proposed scheme. This might be in agreement with the asymmetric shape of the 1090 cm^{-1} Raman band.

This preliminar study of the pure reference phases of the VPO system by laser Raman spectroscopy in catalytic conditions was considered necessary to study the physicochemical characteristics of the VPO catalysts using the same technique. This will be presented in a second paper.

ACKNOWLEDGMENTS

The authors thank Dr. M. Forissier for assistance in the construction of the LRS cell and Mrs. Roullet for calibration of the chromatographic analysis. They also thank the ATOCHEM Co. for financial support.

REFERENCES

1. Delgass, W. N., Haller, G. L., Kellerman, R., and Lunsford, J. H., "Spectroscopy in Heterogeneous Catalysis," p. 58, New York, Academic Press, 1979.
2. Chan, S. S., Wachs, I. E., Murrell, L. L., Wang, L., and Keith Hall, W., *J. Phys. Chem.* **88,** 5381 (1984).
3. Went, G. T., Oyama, S. T., and Bell, A. T., *J. Phys. Chem.* **94,** 4240 (1990).
4. Hardcastle, F. D., and Wachs, I. E., *J. Phys. Chem.* **95,** 5031 (1991).

5. Moser, T. P., and Schrader, G. L., *J. Catal.* **92,** 216 (1985).
6. Lashier, M. E., Moser, T. P., and Schrader, G. L., *in* "Proceedings, Symposium on New Developments in Selective Oxidation" (G. Centi and F. Trifiro, Eds.), Studies in Surface Science and Catalysis, Vol. 55, p. 573, Elsevier, Amsterdam, 1990.
7. Lashier, M. E., and Schrader, G. L., *J. Catal.* **128,** 113 (1991).
8. Hodnett, B. K., *Catal. Rev. Sci. Eng.* **27**(3), 373 (1985).
9. Centi, G., Trifiro, F., Ebner, J. R., and Franchetti, V. M., *Chem. Rev.* **88,** 55 (1988).
10. Harrouch Batis, N., Batis, H., Ghorbel, A., Védrine, J. C., and Volta, J. C., *J. Catal.* **128,** 248 (1991).
11. Bordes, E., *Catal. Today* **1,** 499 (1987).
12. Gopal, R., and Calvo, C., *J. Solid State Chem.* **5,** 432 (1972).
13. Jordan, B., and Calvo, C., *Can. J. Chem.* **51,** 2621 (1973).
14. Linde, S. A., Gorbunova, Yu. E., Lavrov, A. V., and Kuznetsov, V. G., *Dokl. Akad. Nauk SSSR* **245,** 584 (1979).
15. Bordes, E., Johnson, J. W., Raminosona, A., and Courtine, P., *Mater. Sci. Monogr.* **28B,** 887 (1985).
16. Ladwig, G., *Z. Anorg. Chem.* **338,** 266 (1965).
17. Bordes, E., Courtine, P., and Pannetier, G., *Ann. Chim.* **8,** 105 (1973).
18. Bordes, E., and Courtine, P., *J. Catal.* **57,** 236 (1979).
19. Souchay, P., and Dubois, S., *Ann. Chim.* **3,** 88 (1948).
20. Johnson, J. W., Johnston, D. C., Jacobson, A. J., and Brody, J. F., *J. Am. Chem. Soc.* **106,** 8123 (1984).
21. Zimmerer, N., and Kiefer, W., *Appl. Spectrosc.* **28,** 279 (1974).
22. Bhargava, R. N., and Condrate, R. A., *Appl. Spectrosc.* **31,** 230 (1974).
23. Bachmann, H. G., Ahmed, F. R., and Barnes, W. H., *Z. Kristallogr.* **115,** 110 (1961).
24. Abello, L., Husson, E., Repelin, Y., and Lucazeau, G., *Spectrochim. Acta Part A* **39,** 641 (1984).
25. Stranford, G. T., and Condrate, R. A., *Spectrosc. Lett.* **17,** 85 (1984).
26. Stranford, G. T., Ph. D. Thesis, Alfred University, 1988.
27. Tachez, M., Theobald, F., and Bordes, E., *J. Solid State Chem.* **40,** 280 (1981).
28. Tietze, H. R., *Aust. J. Chem.* **34,** 2035 (1981).
29. Ben Abdelouahab, F., Olier, R., and Volta, J. C., *J. Chem. Soc. Faraday Discuss.*, submitted for publication.
30. Preston, C. M., and Adams, W. A., *J. Phys. Chem.* **83,** 814 (1979).